J. Fluid Mech. (2012), *vol.* 695, *pp.* 149–172.
doi:10.1017/jfm.2012.6

A fully adaptive wavelet-based approach to homogeneous turbulence simulation

G. De Stefano[1] **and O. V. Vasilyev**[2]†

[1] Dipartimento di Ingegneria Aerospaziale e Meccanica, Seconda Università di Napoli, I-81031 Aversa, Italy

[2] Department of Mechanical Engineering, University of Colorado, Boulder, CO 80309, USA

(Received 11 February 2011; revised 6 November 2011; accepted 29 December 2011; first published online 8 February 2012)

The ability of wavelet multi-resolution analysis to detect and track the energy-containing motions that govern the dynamics of a fluid flow offers a unique hierarchical framework for modelling and simulating turbulence. In this paper, the role of the wavelet thresholding level in wavelet-based modelling and simulation of turbulent flows is systematically examined. The thresholding level controls the relative importance of resolved energetic structures and residual unresolved background flow and, thus, the achieved *turbulence resolution*. A fully adaptive eddy capturing approach is developed that allows variable-fidelity numerical simulations of turbulence to be performed. The new method is based on wavelet filtering with time-varying thresholding. The thresholding level automatically adapts to the desired *turbulence resolution* during the simulation. The filtered governing equations supplemented by a localized dynamic energy-based closure model are solved numerically using the adaptive wavelet collocation method. The approach is successfully tested in the numerical simulation of both linearly forced and freely decaying homogeneous turbulence.

Key words: homogeneous turbulence, turbulence modelling, turbulence simulation

1. Introduction

Recent advances in wavelet-based numerical methodologies for the solution of partial differential equations, combined with the unique properties of wavelet analysis to identify and isolate localized dynamically dominant flow structures unambiguously, and to track them on adaptive computational meshes, make it feasible to develop *intelligent* methods for turbulent flow simulation that tightly integrate numerics- and physics-based modelling (Schneider & Vasilyev 2010). The centrepiece of this approach is the existence of energetic coherent structures that govern the turbulent flow dynamics across the full spectral range (Vincent & Meneguzzi 1991). The integration of turbulence modelling with adaptive wavelet methods results in a hierarchical approach in which coherent eddies are either totally or partially resolved on self-adaptive computational grids, while possibly modelling the effect of unresolved motions. The separation between resolved (more energetic) eddies and residual (less energetic) flow is achieved by means of a nonlinear wavelet thresholding filter.

† Email address for correspondence: oleg.vasilyev@colorado.edu

The value of wavelet threshold controls the relative importance of resolved field and residual background flow and, thus, the required *turbulence resolution* length scale (Pope 2004).

By varying the thresholding level, a unified hierarchy of wavelet-based turbulence models of different fidelity is obtained. The choice of a sufficiently small threshold for wavelet filtering eliminates the need to do any modelling because the flow field that is filtered out is not significant for the flow dynamics (Sagaut, Deck & Terracol 2006). The resulting approach can be referred to as wavelet-based direct numerical simulation (WDNS). When the threshold is based on the Donoho's denoising procedure (Donoho & Johnstone 1994), the resolved field can be interpreted as the coherent part of the flow, where the residual field is presumed to be Gaussian white noise whose effect was shown to be dynamically insignificant (Goldstein & Vasilyev 2004; Goldstein, Vasilyev & Kevlahan 2005). The corresponding approach has come to be known as coherent vortex simulation (CVS) (Farge, Schneider & Kevlahan 1999). Finally, for higher filtering thresholds, the influence of the residual field on the evolution of the resolved flow cannot be ignored and must be modelled, resulting in the stochastic coherent adaptive large eddy simulation (SCALES) approach (Goldstein & Vasilyev 2004). A number of wavelet-based subgrid-scale (SGS) models for SCALES have recently been introduced, for instance, in De Stefano, Vasilyev & Goldstein (2008) and Vasilyev *et al.* (2008).

The SCALES method is ideal for the simulation of complex turbulent flows since it includes adaptive gridding that allows the energy-containing motions to be resolved, regardless of their position and size, so that the great part of the turbulence energy is captured throughout the physical domain. However, for very complex flows, the dominant scales of motion vary significantly from region to region as well as in time. For this reason, in order to fully exploit the dynamically adaptive nature of wavelet-based methods, the basic idea behind SCALES can be taken one step further by applying a time-dependent wavelet thresholding strategy. In this study, a new wavelet-based approach with time-varying thresholding filter is introduced, while the development of a spatially varying thresholding methodology is the subject of ongoing research. The thresholding level automatically adapts to the desired *turbulence resolution* following the temporal evolution of the dominant flow structures. In this way, a fully adaptive approach to the numerical simulation of homogeneous turbulent flows is obtained.

The rest of the paper is organized as follows. After recalling the basic concept of wavelet threshold filtering in § 2, the general features of the wavelet-based approach to turbulence simulation are briefly reviewed in § 3, with the emphasis on the role played by the wavelet thresholding level. The new time-dependent wavelet thresholding strategy is introduced in § 4. The results of the numerical experiments conducted for both constant and time-varying thresholding are presented in § 5. Finally, conclusions are given in § 6.

2. Wavelet-filtered velocity

In the wavelet-based approach to the numerical simulation of turbulence, the separation between resolved energetic structures and unresolved residual flow is obtained through nonlinear multi-resolution wavelet threshold filtering (WTF). The filtering operator is implicitly defined by applying the wavelet transform to the unfiltered turbulent field, zeroing the wavelet coefficients below a given threshold, say ϵ, and transforming back to the physical space (e.g. Farge *et al.* 1999; Goldstein

& Vasilyev 2004). When applied to the velocity field, the WTF procedure results in its decomposition into two different parts: a coherent more energetic velocity field, and a residual less energetic coherent/incoherent one, i.e. $u_i = \overline{u}_i^{>\epsilon} + u_i'$, where $\overline{u}_i^{>\epsilon}$ stands for the wavelet-filtered velocity at level ϵ.

Formally, the wavelet-filtered velocity field, $\overline{u}_i^{>\epsilon}(\boldsymbol{x})$, is defined by expressing the instantaneous velocity field in terms of wavelet basis functions,

$$u_i(\boldsymbol{x}) = \sum_{\boldsymbol{l}\in\mathscr{L}^0} c_{\boldsymbol{l}}^0 \phi_{\boldsymbol{l}}^0(\boldsymbol{x}) + \sum_{j=0}^{+\infty} \sum_{\mu=1}^{2^n-1} \sum_{\boldsymbol{k}\in\mathscr{K}^{\mu,j}} d_{\boldsymbol{k}}^{\mu,j} \psi_{\boldsymbol{k}}^{\mu,j}(\boldsymbol{x}), \tag{2.1}$$

and retaining only wavelets with significant 'strength':

$$\overline{u}_i^{>\epsilon}(\boldsymbol{x}) = \sum_{\boldsymbol{l}\in\mathscr{L}^0} c_{\boldsymbol{l}}^0 \phi_{\boldsymbol{l}}^0(\boldsymbol{x}) + \sum_{j=0}^{+\infty} \sum_{\mu=1}^{2^n-1} \sum_{\substack{\boldsymbol{k}\in\mathscr{K}^{\mu,j} \\ |d_{\boldsymbol{k}}^{\mu,j}|>\epsilon\|u_i\|_{WTF}}} d_{\boldsymbol{k}}^{\mu,j} \psi_{\boldsymbol{k}}^{\mu,j}(\boldsymbol{x}). \tag{2.2}$$

In the above decomposition, bold subscripts denote n-dimensional indices, while $\mathscr{L}^0$ and $\mathscr{K}^{\mu,j}$ are n-dimensional index sets associated with scaling functions at zero level of resolution ($\phi_{\boldsymbol{l}}^0$) and wavelets of family μ and level j ($\psi_{\boldsymbol{k}}^{\mu,j}$), respectively. Each level of resolution j consists of a family of wavelets $\psi_{\boldsymbol{k}}^{\mu,j}$ having the same scale but located at different grid positions. In practice, a wavelet $\psi_{\boldsymbol{k}}^{\mu,j}$ whose coefficient is below the given threshold is discarded when the turbulent velocity field has no significant variation at the jth level of resolution in the immediate vicinity of the corresponding wavelet collocation point. In a real calculation, the maximum value for j (which corresponds to the highest level of resolution) is dictated by the acceptable computational cost. Depending on the choice of the WTF level ϵ, only a relatively small number of wavelets are actually retained in representing the filtered field $\overline{u}_i^{>\epsilon}$, which leads to the characteristic compression property of wavelet-based methods. In this study, the L_2 norm is assumed as WTF norm and, dealing with homogeneous turbulence, the same scaling is used in all directions, i.e. $\|u_i\|_{WTF} \cong \|\overline{u}_i^{>\epsilon}\|_{WTF} = (2\mathscr{K}_{res})^{1/2}$, where $\mathscr{K}_{res} = \langle (1/2)\overline{u}_j^{>\epsilon}\,\overline{u}_j^{>\epsilon}\rangle$ stands for the volume-averaged resolved kinetic energy.

The key role in the wavelet-filter definition is clearly played by the non-dimensional relative thresholding level ϵ that explicitly defines the relative energy level of the eddies that are resolved and, consequently, controls the importance of the influence of the residual field on the dynamics of the resolved motions. It is worth stressing that the dimensional absolute thresholding scale, which is evaluated as $\epsilon\|\overline{u}_i^{>\epsilon}\|_{WTF}$, actually varies in time following the evolution of the turbulent velocity field.

The high compression property of the wavelet-based decomposition is illustrated in table 1, where the percentage of active wavelets and retained energy/enstrophy are reported as a function of the WTF level for a given instantaneous turbulent velocity field. The field considered is a realization of a statistically stationary turbulent flow at $Re_\lambda = 72$ (λ being the Taylor microscale) as provided by a pseudo-spectral direct numerical simulation (DNS) solution (De Stefano, Goldstein & Vasilyev 2005). For instance, by retaining less than 0.5 % of the available 256^3 wavelets, more than 98 % of the energy and 77 % of the DNS enstrophy are captured (as happens for $\epsilon = 0.40$). Also, the use of a very low but non-zero threshold allows practically the entire energy/enstrophy content of the flow to be retained (as happens for $\epsilon = 0.05$).

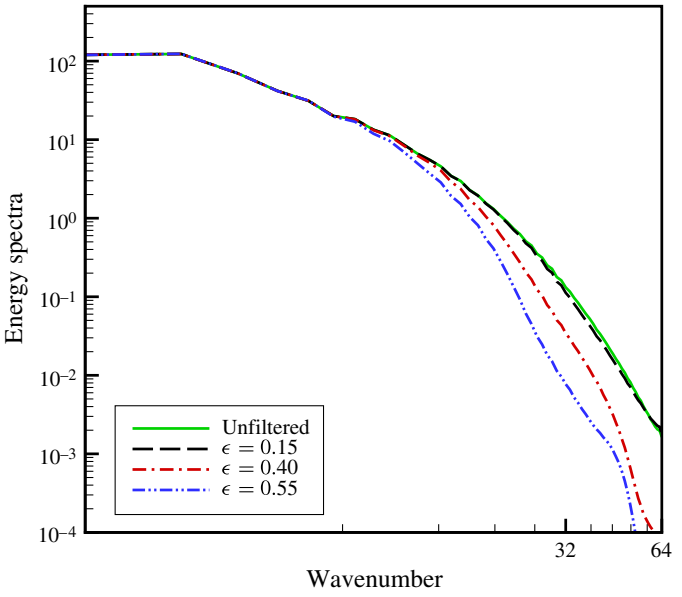

FIGURE 1. (Colour online available at journals.cambridge.org/flm) Energy spectra for wavelet-filtered instantaneous velocity with different thresholding levels ($\epsilon = 0.15$, 0.40 and 0.55), along with the unfiltered solution.

Level ϵ	Wavelets (%)	Energy (%)	Enstrophy (%)
0.55	0.15	95.08	60.06
0.40	0.46	98.11	77.08
0.15	5.07	99.88	97.53
0.05	12.50	99.99	99.98

TABLE 1. Percentage of active wavelets and captured energy/enstrophy for different thresholding levels.

Another important feature of wavelet filtering is the ability to capture coherent energetic eddies of any size so that the small-scale turbulence can be represented, at least partially, by the wavelet-filtered field. This is illustrated in figure 1, where the energy spectrum of the filtered velocity field is reported for different filtering levels. This property is distinctively different from typical filtering adopted in classical non-adaptive large eddy simulation (LES), where the small dissipative scales are not resolved at all.

3. Adaptive wavelet-based simulation

The space–time evolution of the wavelet-filtered turbulent velocity is simulated by numerically solving the wavelet-filtered Navier–Stokes equations, possibly supplied with a suitable closure model. In this section, the conceptual steps that form the adaptive wavelet-based methodology are briefly reviewed. The details of the SCALES procedure can be found, for example, in Goldstein & Vasilyev (2004).

3.1. *Wavelet-filtered Navier–Stokes equations*

The governing equations for wavelet-based adaptive simulation of incompressible turbulent flows are formally obtained by applying the WTF operator, implicitly given by (2.1) and (2.2), to the Navier–Stokes equations, followed by the divergence-free projection. For forced turbulence, the equations are written as

$$\frac{\partial \overline{u}_i^{>\epsilon}}{\partial x_i} = 0, \tag{3.1}$$

$$\frac{\partial \overline{u}_i^{>\epsilon}}{\partial t} + \overline{u}_j^{>\epsilon} \frac{\partial \overline{u}_i^{>\epsilon}}{\partial x_j} = -\frac{1}{\rho} \frac{\partial \overline{p}^{>\epsilon}}{\partial x_i} + \nu \frac{\partial^2 \overline{u}_i^{>\epsilon}}{\partial x_j \partial x_j} - \frac{\partial \tau_{ij}}{\partial x_j} + \overline{f}_i^{>\epsilon}, \tag{3.2}$$

where ρ and ν are the constant density and kinematic viscosity of the fluid, while f_i stands for the unfiltered forcing field. Note that the bar symbol in the notation of the pressure variable, $\overline{p}^{>\epsilon}$, does not imply the application of the WTF operator, but is used for consistency with the other terms. Actually, the pressure term in the filtered momentum equation must be viewed as a Lagrange multiplier enforcing the incompressibility constraint.

The application of the WTF operator to the Navier–Stokes equations also results in the appearance of the unresolved quantities

$$\tau_{ij} = \overline{u_i u_j}^{>\epsilon} - \overline{u}_i^{>\epsilon} \overline{u}_j^{>\epsilon}, \tag{3.3}$$

commonly referred to as SGS stresses. The residual SGS stresses can be thought of as representing the effect of unresolved less energetic background flow on the dynamics of the resolved energetic eddies. In order to close the equations, an SGS model is required to express the unknown stresses (3.3) as a given function of the resolved velocity field $\overline{u}_i^{>\epsilon}$. In practice, the isotropic part of the SGS stress tensor being incorporated by a modified filtered pressure variable, only the deviatoric part, hereafter denoted with a star, $\tau_{ij}^* = \tau_{ij} - (1/3)\tau_{kk}\delta_{ij}$, is actually modelled in incompressible SCALES. When dealing with forced turbulence, the SGS model is mainly required to provide the right amount of energy dissipation that – once added to the resolved viscous dissipation – allows the energy content of the flow to be maintained statistically constant in time. The importance of the local SGS dissipation, which is defined as $\Pi_{sgs} = -\tau_{ij}^* \overline{S}_{ij}^{>\epsilon}$, where $\overline{S}_{ij}^{>\epsilon} = (1/2)(\partial \overline{u}_i^{>\epsilon}/\partial x_j + \partial \overline{u}_j^{>\epsilon}/\partial x_i)$ is the resolved filtered rate-of-strain tensor, is expected to increase with the thresholding level ϵ.

From the mathematical point of view, once a model for the SGS stress tensor is given and suitable initial conditions are provided, the SCALES governing equations can be solved using any numerical method. In practice, (3.2) is solved using the dynamically adaptive wavelet collocation method (AWCM), where the same wavelet-filtering procedure with the same wavelet threshold is exploited to automatically adapt the computational grid to the numerical solution, in both location and scale (e.g. Vasilyev & Bowman 2000; Vasilyev 2003). Owing to the existing one-to-one correspondence between wavelet coefficients and grid points that is induced by the discretization of the physical domain, the thresholding level ϵ also controls the dynamic mesh adaptation and, thus, the numerical accuracy of the solution. Regarding the time-integration procedure, a multi-step pressure correction method is employed for the integration of (3.2) with the continuity constraint (3.1) (Kevlahan & Vasilyev 2005). The resulting Poisson equation is solved using the AWCM elliptic solver developed in Vasilyev & Kevlahan (2005).

Additionally, it should be mentioned that, as in LES with non-uniform filter width (Vasilyev, Lund & Moin 1998; Marsden, Vasilyev & Moin 2002; Haselbacher & Vasilyev 2003), there is a commutation error between WTF and differential operators, the effect of which is not considered in this work. However, since the grid adaption makes use of an adjacent zone, which also includes wavelets with smaller coefficients that can possibly become significant during the single time step (e.g. Schneider & Vasilyev 2010), the commutation error is significantly reduced.

3.2. *Wavelet-based SGS model*

In this work, the unknown SGS stresses are approximated by means of the localized dynamic kinetic-energy-based model (LDKM) recently developed for SCALES. The main steps of the modelling procedure are briefly outlined in this section, while the details can be found in De Stefano *et al.* (2008). The filtered momentum equation (3.2) is closed using the classical eddy-viscosity assumption, with the turbulent viscosity expressed in terms of the SGS kinetic energy k_{sgs} and the wavelet-filter characteristic width Δ, that is

$$\tau_{ij}^{*} \cong -2C_{\nu}\Delta k_{sgs}^{1/2}\overline{S}_{ij}^{>\epsilon}. \tag{3.4}$$

In the above equation, the dimensionless model coefficient $C_{\nu}(\boldsymbol{x}, t)$ is dynamically evaluated during the calculation following a Germano-like approach. The non-uniform time-dependent filter width $\Delta(\boldsymbol{x}, t)$ is determined from knowledge of the actual wavelet mask used in the simulation. This parameter, which closely reflects the prescribed thresholding level, actually stands for the *turbulence resolution* length scale in the SCALES approach.

The space–time evolution of the SGS energy $k_{sgs}(\boldsymbol{x}, t) = (1/2)(\overline{u_i u_i}^{>\epsilon} - \overline{u}_i^{>\epsilon}\overline{u}_i^{>\epsilon})$ is simulated by solving the following additional model equation, as proposed in Ghosal *et al.* (1995),

$$\frac{\partial k_{sgs}}{\partial t} + \overline{u}_j^{>\epsilon}\frac{\partial k_{sgs}}{\partial x_j} = \nu\frac{\partial^2 k_{sgs}}{\partial x_j \partial x_j} - \varepsilon_{sgs} + \Pi_{sgs}. \tag{3.5}$$

This equation accounts for the energy transfer back and forth between resolved and unresolved eddies, as well as for the viscous dissipation of SGS energy,

$$\varepsilon_{sgs} = \nu\left(\overline{\frac{\partial u_i}{\partial x_j}\frac{\partial u_i}{\partial x_j}}^{>\epsilon} - \frac{\partial \overline{u}_i^{>\epsilon}}{\partial x_j}\frac{\partial \overline{u}_i^{>\epsilon}}{\partial x_j}\right), \tag{3.6}$$

which is approximated following a Bardina-like approach.

The wavelet-filtered Navier–Stokes equations (3.2) and the SGS kinetic energy equation (3.5) stand for a set of coupled equations that is solved with the AWCM approach mentioned in § 3.1. Note that the cost associated with the use of an additional equation is minimal due to the vectorized form of the wavelet transform and differential operators utilized by the solver. Furthermore, it is practically negligible compared to the computational cost of solving the elliptic problem for the pressure correction.

According to model (3.4), the SGS dissipation is approximated as

$$\Pi_{sgs} \cong C_{\nu}\Delta k_{sgs}^{1/2}\,|\overline{S}^{>\epsilon}|^2, \tag{3.7}$$

where $|\overline{S}^{>\epsilon}| = (2\overline{S}_{ij}^{>\epsilon}\overline{S}_{ij}^{>\epsilon})^{1/2}$ is the characteristic filtered rate of strain. The magnitude of the SGS energy and, thus, the importance of the modelled dissipation increase with

the wavelet-filtering threshold ϵ. This is confirmed by the results shown in § 5. It is worth noting that the above wavelet-based SGS model inherently acts as a multiscale dynamic model since, by definition, each wavelet level in WTF decomposition (2.2) corresponds to a broad range in wavenumber space.

4. Time-varying thresholding method

Prior to this work, all SCALES simulations (e.g. Goldstein & Vasilyev 2004; De Stefano & Vasilyev 2010) were conducted with *a priori* fixed level of threshold parameter, resulting in a subjective separation of resolved and unresolved flow structures. However, when dealing with complex turbulent flows, the energy content of the dominant flow structures can significantly vary in time, so that the desired level of *turbulence resolution* cannot be maintained with constant thresholding level. In fact, the level ϵ at which decomposition (2.2) is truncated should be consistent with the actual flow conditions and, thus, variable.

In order to develop a fully adaptive approach, in this work, the basic idea behind SCALES is taken one step further by applying a time-dependent wavelet thresholding method. With this new strategy, the wavelet filtering threshold ϵ is not prescribed but is determined on the fly, as a time-dependent function, for a given desired level of *turbulence resolution*.

The latter can be measured, for instance, by the ratio between the modelled dissipation and the sum of resolved and modelled dissipations, i.e.

$$\mathscr{R}(t) = \frac{\mathscr{D}_{sgs}}{\mathscr{D}_{res} + \mathscr{D}_{sgs}}, \tag{4.1}$$

where $\mathscr{D}_{sgs} = \langle C_\nu \Delta k_{sgs}^{1/2} |\overline{S}^{>\epsilon}|^2 \rangle$ stands for the volume-averaged modelled SGS dissipation, while $\mathscr{D}_{res} = \langle \nu |\overline{S}^{>\epsilon}|^2 \rangle$ represents the volume-averaged resolved viscous dissipation.

The definition (4.1), which corresponds to the 'subgrid activity' parameter introduced in Geurts & Fröhlich (2002), provides an objective measure that can be used to classify and compare LES solutions. This parameter has been extensively used to analyse and develop SGS modelling procedures (e.g. Meyers & Sagaut 2006). Since the net energy transfer is from resolved to unresolved motions, it holds that $0 < \mathscr{R} < 1$. Along this line of argument, prescribing the desired *turbulence resolution* is equivalent to assigning a goal value for the ratio (4.1). For statistically steady turbulence, the total dissipation $\mathscr{D}_{res} + \mathscr{D}_{sgs}$ can be assumed given and known, so that the magnitude of $\mathscr{R}$ directly links to that of $\mathscr{D}_{sgs}$ and, thus, to the wavelet thresholding level, which can be viewed as the control parameter for the *turbulence resolution*. The smaller the value of ϵ, the smaller the fraction of energy dissipation that is modelled and, thus, the smaller the value of $\mathscr{R}$.

Hence, the thresholding level $\epsilon(t)$ can be evolved in time according to the simple feedback control equation

$$\frac{\mathrm{d}\epsilon}{\mathrm{d}t} = -(\mathscr{R} - \mathscr{R}_0)\frac{\epsilon}{\tau_\epsilon}, \tag{4.2}$$

where $\mathscr{R}_0$ is the goal value corresponding to the desired level of resolution and τ_ϵ is a suitable relaxation time parameter. In practice, when the grid is too coarse, i.e. when the SGS dissipation provided by the model is higher than the goal ($\mathscr{R} > \mathscr{R}_0$), the threshold value decreases, which automatically results in increasing the grid resolution and, thus, reducing the SGS dissipation level. On the contrary, when the turbulence

is over-resolved, i.e. the SGS dissipation is too low ($\mathscr{R} < \mathscr{R}_0$), the threshold value increases, resulting in the mesh coarsening that leads to higher SGS dissipation.

Equation (4.2) is explicitly discretized and solved step by step in time along with the filtered governing equations (3.2) and (3.5), starting from a given initial value $\epsilon(0) = \epsilon_0$. The relaxation time constant τ_ϵ must be linked to some characteristic time scale of the turbulent flow under simulation. For example, this parameter can be chosen as a given fraction of the characteristic eddy turnover time of the turbulence, when it is known. In this work, another possibility is successfully tested by considering the time scale associated with the volume-averaged characteristic filtered rate of strain,

$$\frac{1}{\tau_\epsilon} = \left\langle \left| \overline{S}^{>\epsilon} \right| \right\rangle . \tag{4.3}$$

In this way, the relaxation parameter by itself dynamically adapts to the instantaneous flow conditions. Note that, in the homogeneous turbulence case, the proposed feedback mechanism (4.2) effectively controls the level of SGS dissipation. A similar approach can be utilized to control any other suitable error measure that can be used for more complex flows (e.g. Terracol, Sagaut & Basdevant 2003).

As an alternative to definition (4.1), while using the SGS energy-based model presented in § 3.2, the *turbulence resolution* could also be measured by the ratio of SGS to resolved kinetic energy, i.e. $\mathscr{K}_{sgs}/\mathscr{K}_{res}$, where $\mathscr{K}_{sgs} = \langle k_{sgs} \rangle$ stands for the volume-averaged SGS energy. Consequently, the desired resolution would be prescribed by assigning a goal value for this ratio. However, since not all SCALES models exploit the SGS kinetic energy definition, this choice appears less robust. Moreover, it could be not well founded and is somewhat subjective because the variable k_{sgs} mostly acts as a feedback parameter, whose level might differ from the true energy of the SGS eddies. For these reasons, this possibility is not explored in the following experiments.

It is worth stressing that the dynamically adaptive nature of wavelet methods is fully exploited by adopting the present time-dependent wavelet-filtering thresholding strategy. Following Pope (2004), the corresponding methodology can be referred to as a 'complete' large eddy simulation approach to the numerical simulation of homogeneous turbulent flows.

5. Numerical experiments

In order to carry out some numerical experiments, the simulation of forced incompressible homogeneous turbulence is considered. Following the linear forcing scheme of Lundgren (2003), the forcing term in (3.2) is assumed proportional to the velocity field, $\overline{f}_i^{>\epsilon} = Q\overline{u}_i^{>\epsilon}$, where Q stands for a constant parameter. In fact, fixing this parameter is equivalent to prescribing the eddy turnover time of the turbulence, since, for statistically steady turbulent flows,

$$\tau_{eddy} = \frac{u'^2}{\langle \varepsilon \rangle} = \frac{1}{3Q}, \tag{5.1}$$

where $u' = (2\mathscr{K}_{res}/3)^{1/2}$ stands for the root mean square velocity and $\langle \varepsilon \rangle$ is the volume-averaged turbulent dissipation (Rosales & Meneveau 2005). In this study, in order to make a useful comparison, the same linear forcing coefficient $Q = 5.2$ adopted in De Stefano & Vasilyev (2010) is considered.

All the simulations presented in the following sections start from the same initial velocity field. The latter is a realization of a statistically steady linearly forced flow at $Re_\lambda = 60$ (λ being the Taylor microscale) that is provided by a fully de-aliased pseudo-spectral 192^3 DNS solution for the unfiltered Navier–Stokes equations (De Stefano *et al.* 2005). The corresponding pseudo-spectral code with the same Fourier grid is used to produce a reference DNS solution (hereafter denoted as SDNS) for the present experiments.

Owing to the finite-difference nature of the AWCM solver, in order to have a meaningful comparison, the grid resolution is increased with respect to the spectral case. Wavelet-based numerical solutions are obtained using a maximum resolution corresponding to 256^3 wavelet collocation points. In fact, the actual number of wavelets used in the simulation is very low with respect to the maximum value, thanks to the high compression property of the wavelet-based methods.

It should be noted that the time histories of the forcing term for SCALES, CVS, WDNS and SDNS are not exactly the same. This fact unavoidably leads to some discrepancies in the solutions. The possibility of addressing the issue by applying the linear force in Fourier space for a given shell of small wavenumbers, as done, for instance, in Machiels (1997), is not considered here, owing to the use of an adaptive computational mesh by the finite-difference-based wavelet solver. However, DNS remains the natural reference solution for the present calculations, as happens for classical non-adaptive LES, even when the turbulence is forced in the entire wavenumber domain (e.g. Rosales & Meneveau 2005). Furthermore, since wavelet-based solutions capture most of the energy and enstrophy spectra (Goldstein & Vasilyev 2004; Goldstein *et al.* 2005), the difference in forcing is considerably smaller than for non-adaptive LES.

5.1. *Constant thresholding*

As discussed in the previous sections, wavelet-based approaches with different fidelity are obtained by choosing different thresholding levels in WTF definition (2.2). In order to address the effect of such a choice systematically, the results of simulations with different constant thresholding levels are presented. The tested levels are also chosen by comparison with previous studies carried out for decaying homogeneous turbulence (e.g. De Stefano *et al.* 2008). This *a posteriori* study is the natural continuation of the *a priori* analysis conducted in § 2, where the effect of wavelet filtering upon the instantaneous velocity field is considered. The simulation of steady forced turbulence allows the robustness of wavelet decomposition to be examined in terms of the long-term evolution of the filtered Navier–Stokes equations.

When the thresholding level is too high, like for $\epsilon = 0.55$, a poor solution to the filtered governing equations is obtained because the dynamically dominant flow structures are not fully resolved. Besides the fact that the velocity field is strongly distorted by wavelet threshold filtering, the numerical accuracy of the AWCM solution by itself is affected by the inadequate resolution. Moreover, asking the model to provide a great part of energy dissipation that is not resolved is unrealistic. On the other hand, when the threshold is too low, like for $\epsilon = 0.15$, the filtered-velocity field appears over-resolved, a great number of wavelets being retained in the calculation, and the computational cost is comparable to DNS. In this case, the high potential of the dynamic model is under-exploited. A typical SCALES solution is finally obtained for $\epsilon = 0.40$, which represents a good compromise between acceptable numerical accuracy and affordable computing cost, the model providing about 35 % of the total dissipation on average.

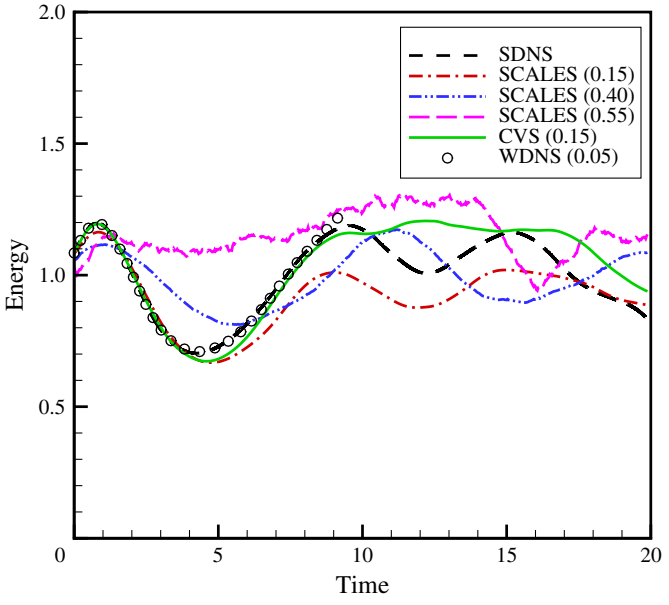

FIGURE 2. (Colour online) Resolved energy for SCALES with different constant thresholding levels ($\epsilon = 0.15$, 0.40 and 0.55), along with the no-model CVS ($\epsilon = 0.15$) and WDNS ($\epsilon = 0.05$) solutions. The reference SDNS solution is shown for comparison.

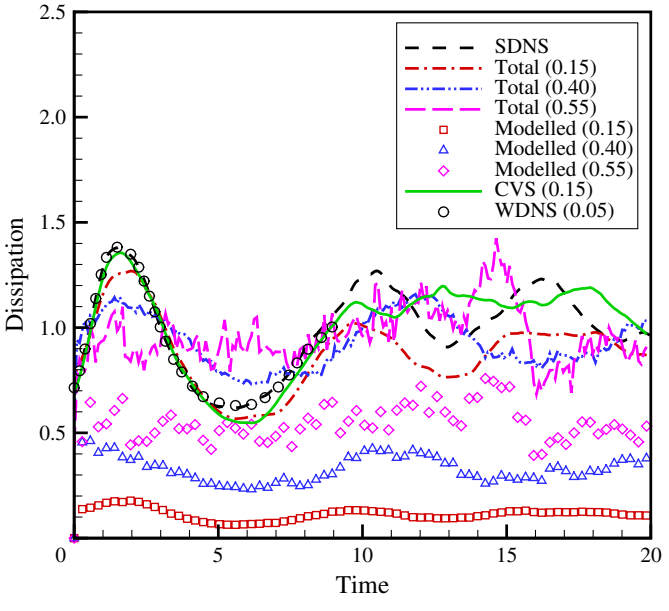

FIGURE 3. (Colour online) Modelled/total dissipation for SCALES with different constant thresholding levels ($\epsilon = 0.15$, 0.40 and 0.55), along with the no-model CVS ($\epsilon = 0.15$) and WDNS ($\epsilon = 0.05$) solutions. The reference SDNS solution is shown for comparison.

The above discussion is corroborated by the inspection of time histories of energy and energy dissipation reported in figures 2 and 3, respectively, for the different

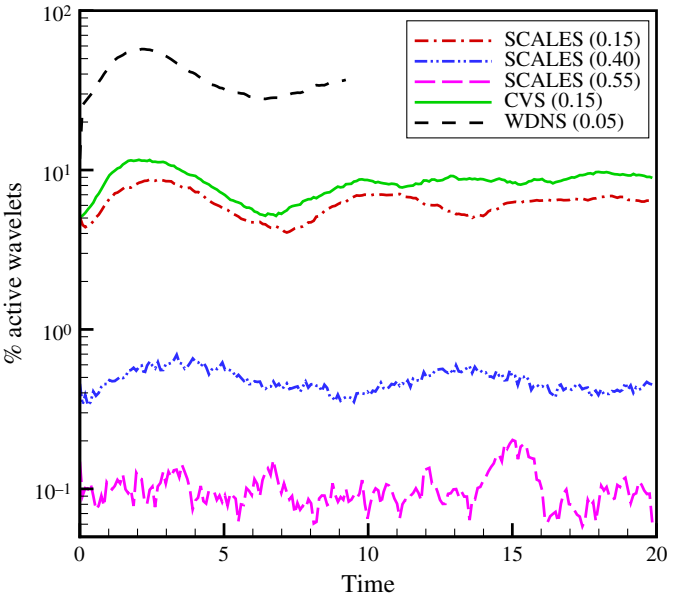

FIGURE 4. (Colour online) Percentage of active wavelets (in logarithmic scale) for SCALES with different constant thresholding levels ($\epsilon = 0.15$, 0.40 and 0.55), along with the no-model CVS ($\epsilon = 0.15$) and WDNS ($\epsilon = 0.05$) solutions.

thresholding levels. The time variable is non-dimensionalized by the theoretical eddy turnover time (5.1), while the dependent variables are non-dimensionalized by the corresponding time-averaged reference SDNS data. The analysis is conducted for a time interval corresponding to 20 eddy turnover times. As shown in the figures, when the threshold value is adequate, the adaptive solution is able to follow – at least partially – the physical time evolution of the DNS solution. The results confirm that the contribution of the modelled dissipation grows with increase of ϵ. Also, the lower level of SGS dissipation is associated with the larger fraction of resolved viscous dissipation as well as increased grid resolution. That is clear by looking at the grid compression illustrated in figure 4, where the percentage of retained wavelets is reported in logarithmic scale. A typical SCALES solution involves less than 1 % of the 256^3 available wavelet collocation points, as happens for $\epsilon = 0.40$. As to the spectral distribution of resolved energy, in figure 5 the time-averaged energy spectra are depicted, demonstrating how the capability of the SCALES method in representing small-scale turbulence is maintained during the simulation. Once again, the deficiency of high thresholding levels such as $\epsilon = 0.55$ is clearly demonstrated.

It is illustrative to consider SCALES simulations with relatively low value of threshold parameter, i.e. $\epsilon = 0.15$. This threshold was empirically chosen in Goldstein *et al.* (2005) to conduct CVS of freely decaying isotropic turbulence at $Re_\lambda = 72$. In order to make an interesting comparison with modelled solutions, a simulation with this threshold without any modelling is performed in the linearly forced case. As shown in figures 2, 3 and 5, the results agree well with reference SDNS, even though this no-model solution cannot be strictly considered as CVS. This case demonstrates how the lack (or the inadequacy) of SGS modelling is automatically compensated by locally increasing the resolution and, consequently, the number of grid points used in the simulation, as illustrated in figure 4.

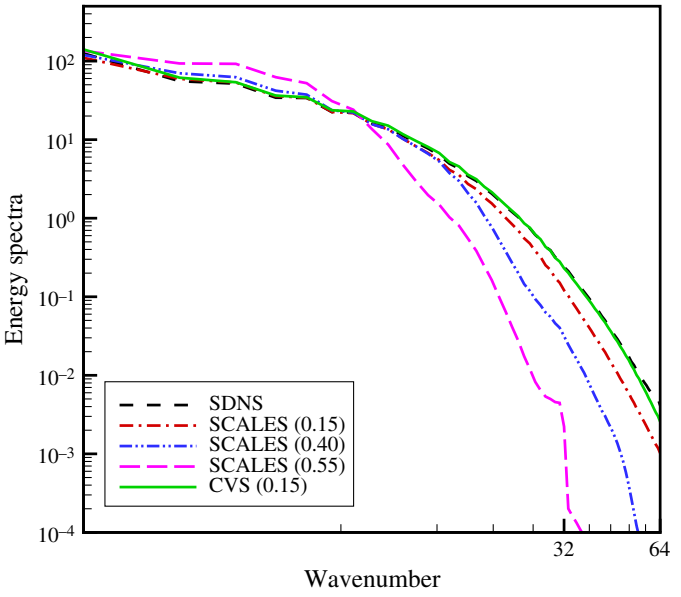

FIGURE 5. (Colour online) Time-averaged energy spectra for SCALES with different constant thresholding levels ($\epsilon = 0.15$, 0.40 and 0.55), along with the no-model CVS solution ($\epsilon = 0.15$). The reference SDNS spectrum is shown for comparison.

For very low threshold values, the direct numerical solution of (3.2) without any model can be thought of as WDNS. In this work, the thresholding level $\epsilon = 0.05$ is assumed to be sufficiently low for direct numerical simulations. Owing to its high computational cost, WDNS is performed for only eight non-dimensional time units. In fact, as illustrated in figure 4, on average about 40 % of the available wavelets are used in this case. The agreement between WDNS and reference SDNS is almost perfect, as demonstrated, for instance, by examining the resolved energy and viscous dissipation depicted in figures 2 and 3, respectively. Even more meaningfully, the agreement holds in the entire wavenumber range, that is, at all flow scales. This is demonstrated, for instance, by inspection of the instantaneous energy spectra at two different (non-dimensional) time instants, which are $t = 4.7$ and $t = 7.8$, reported in figure 6.

5.2. *Time-varying thresholding*

In this section, the practical implementation of the method introduced in § 4 is illustrated, by presenting the results of numerical experiments carried out with time-varying thresholding. The efficiency of the method is first demonstrated by performing SCALES with two very different initial thresholding levels, $\epsilon_0 = 0.60$ and 0.20, respectively, while prescribing the same goal value $\mathscr{R}_0 = 0.40$ for the ratio of modelled to total dissipation (4.1). When starting with a very high threshold like $\epsilon_0 = 0.60$, the resolution is initially too low and the SGS dissipation provided by the model is too high ($\mathscr{R} > \mathscr{R}_0$), so that, according to (4.2), the threshold tends to decrease. The solution with a very low initial threshold like $\epsilon_0 = 0.20$ shows the opposite behaviour because the initial resolution is too high with respect to the goal. In figure 7 the evolution of the wavelet thresholding level is reported for both solutions for a time corresponding to just two non-dimensional time units to make it possible to examine

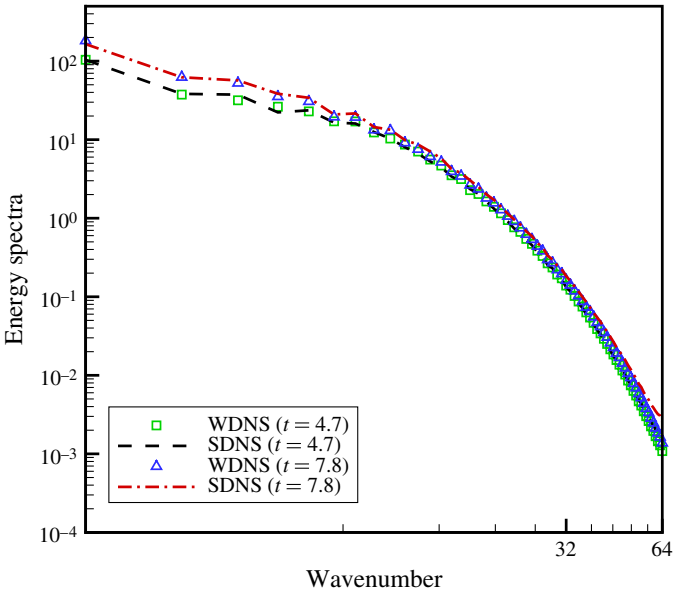

FIGURE 6. (Colour online) Instantaneous energy spectra at two different time instants ($t = 4.7$ and 7.8) for WDNS ($\epsilon = 0.05$) compared to reference SDNS.

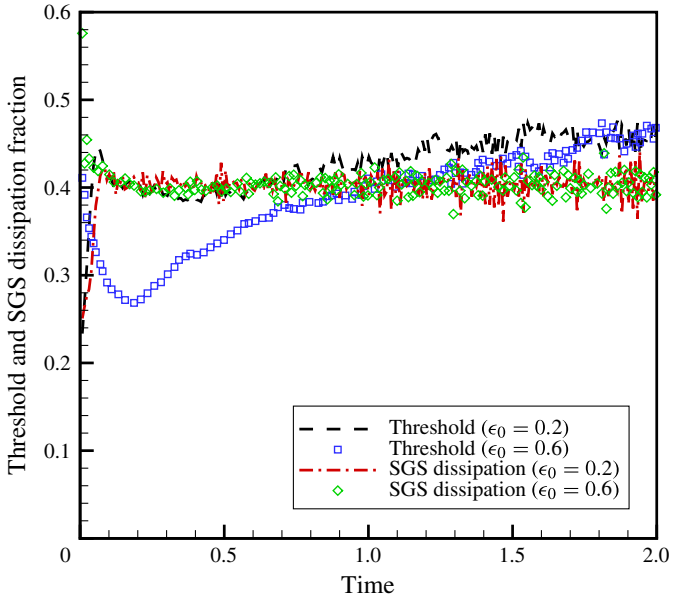

FIGURE 7. (Colour online) Time history of thresholding level and SGS dissipation fraction for SCALES with time-varying thresholding and two different initial conditions ($\epsilon_0 = 0.20$ and 0.60).

the short initial transient in detail. By looking at the time history of the SGS to total dissipation ratio, which is depicted in the same figure, the SCALES solution tends to achieve the prescribed resolution, regardless of the initial thresholding level. For both

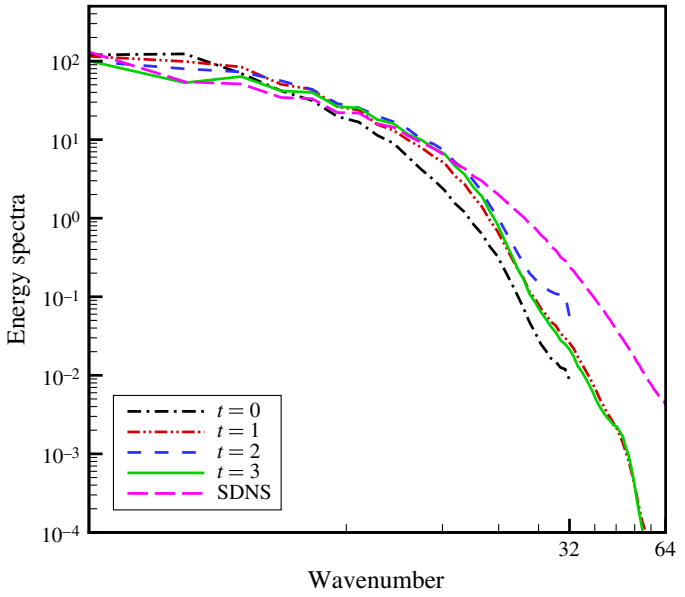

FIGURE 8. (Colour online) Time evolution of energy spectra for SCALES with time-varying thresholding and initial threshold $\epsilon_0 = 0.60$. The reference SDNS time-averaged energy spectrum is shown for comparison.

initial conditions, the transient time is very short, less than half the eddy turnover time of the turbulence. Furthermore, the change from one state to another is faster for the solution with higher initial resolution, since the achievement of the desired goal is easier starting from a finer wavelet collocation grid.

The transition from the initial resolution towards the desired one is well represented by the corresponding evolution of the energy spectra, shown in figures 8 and 9, for the two different initial levels, respectively, along with the reference SDNS time-averaged energy spectrum, which is reported for comparison. For $\epsilon_0 = 0.60$, where the *turbulence resolution* is initially insufficient, smaller scales are automatically created in the simulation as time passes, while the energy spectrum adjusts to the expected shape for linearly forced turbulence (Rosales & Meneveau 2005). Note that, when there are no retained wavelets at the finest levels of resolution, the energy spectra are truncated at wavenumber 32. In contrast, for $\epsilon_0 = 0.20$, where the turbulence is initially over-resolved, the energy associated with the smallest scales reduces as the calculation goes on. Note that the energy spectra after three time units are practically the same for the two different solutions, which can be thought of – from this time forwards – as two different realizations of the same numerical solution with the prescribed resolution. In fact, the two solutions show practically the same behaviour over long-time integration, as demonstrated, for instance, by looking at the energy dissipation reported in figure 10. The constraint $\mathscr{R}_0 = 0.40$ is evidently obeyed while constantly using less than 0.5% of the wavelet collocation points.

The time-varying thresholding strategy is further analysed by performing different simulations for different prescribed ratios of modelled to total dissipation, ranging from $\mathscr{R}_0 = 0.20$ to 0.50, while starting with the same initial thresholding level, $\epsilon_0 = 0.20$. The time evolution of resolved energy and time-averaged energy spectra are depicted for the different solutions in figures 11 and 12, respectively. Consistently with

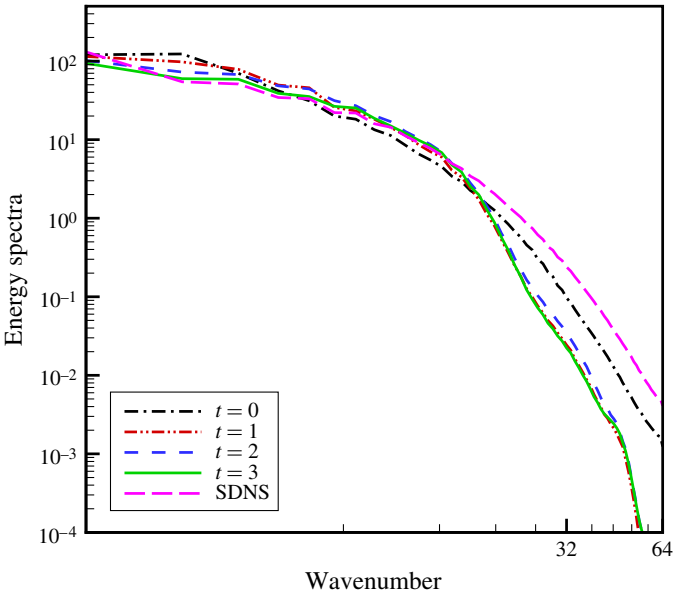

FIGURE 9. (Colour online) Time evolution of energy spectra for SCALES with time-varying thresholding and initial threshold $\epsilon_0 = 0.20$. The reference SDNS time-averaged energy spectrum is shown for comparison.

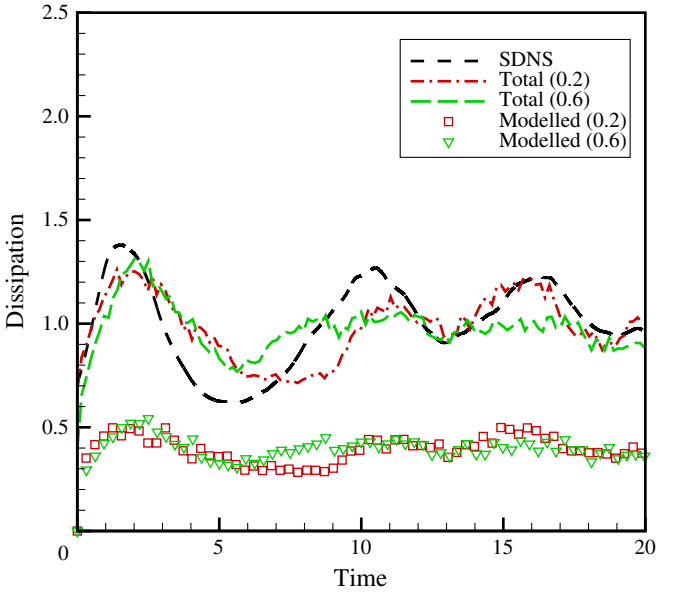

FIGURE 10. (Colour online) Modelled/total dissipation for SCALES with time-varying thresholding and two different initial conditions ($\epsilon_0 = 0.20$ and 0.60). The reference SDNS dissipation is shown for comparison.

the discussion in the previous section, when the prescribed resolution is too coarse, like for $\mathscr{R}_0 = 0.50$, the turbulence appears under-resolved, as is clearly apparent, for

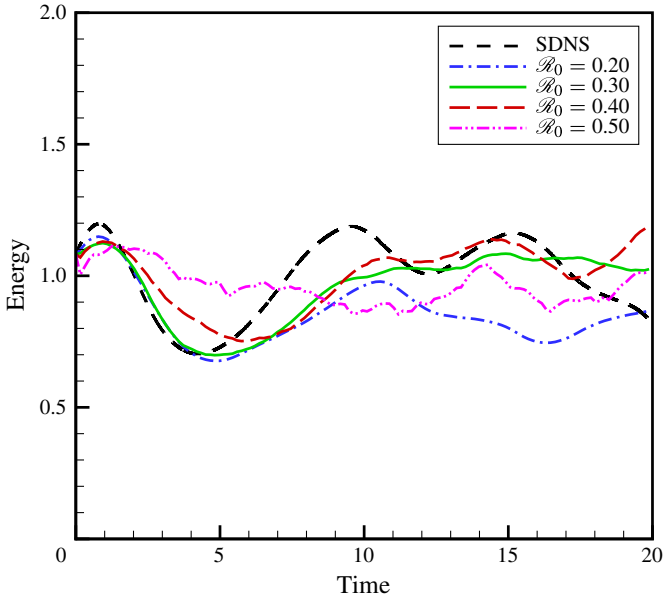

FIGURE 11. (Colour online) Time history of resolved energy for SCALES with time-varying thresholding and different prescribed resolutions ($\mathscr{R}_0 = 0.20$, 0.30, 0.40 and 0.50). The reference SDNS solution is shown for comparison.

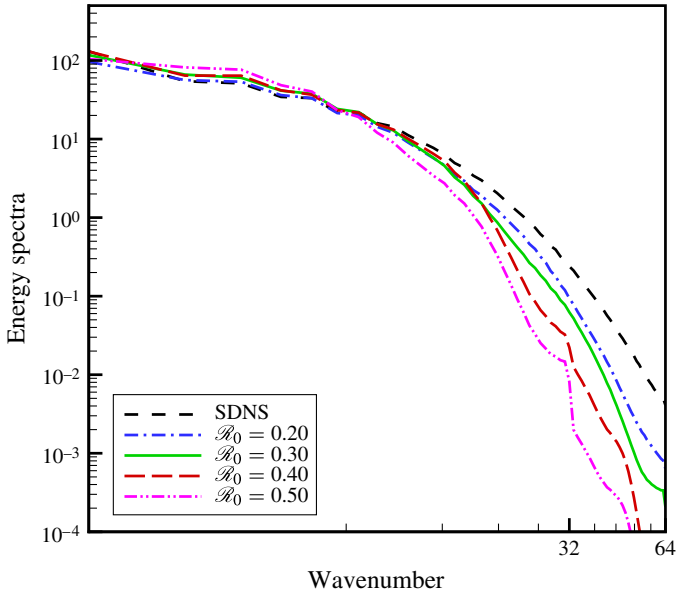

FIGURE 12. (Colour online) Time-averaged energy spectra for SCALES with time-varying thresholding and different prescribed resolutions ($\mathscr{R}_0 = 0.20$, 0.30, 0.40 and 0.50). The reference SDNS solution is shown for comparison.

instance, by looking at the energy spectral distribution at large scales. For this reason, this poor solution is not reported in the following figures.

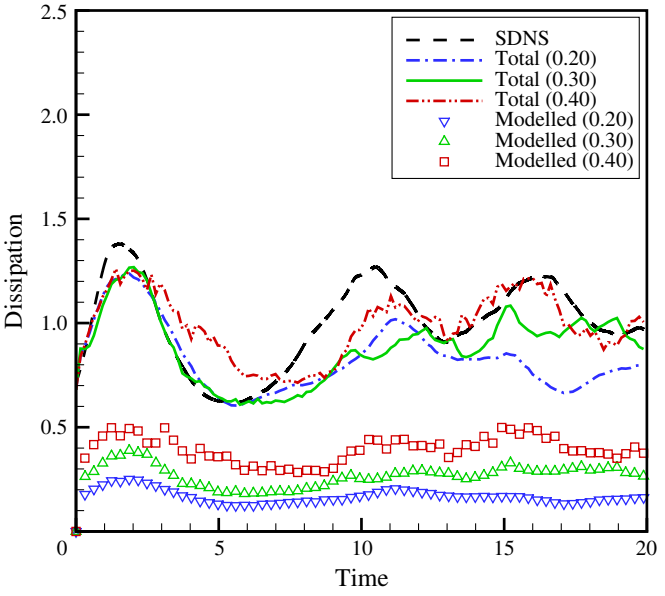

FIGURE 13. (Colour online) Modelled/total dissipation for SCALES with time-varying thresholding and different prescribed resolutions ($\mathscr{R}_0 = 0.20$, 0.30 and 0.40). The reference SDNS solution is shown for comparison.

The time history of modelled and total dissipation for different prescribed resolutions is shown in figure 13, while the time-averaged spectral distribution of resolved viscous dissipation is illustrated in figure 14. It is worth noting that the average level of total dissipation is the same for the different solutions, regardless of the different contributions provided by the model. Furthermore, when looking at the different contributions to total dissipation for a given prescribed goal $\mathscr{R}_0$, it is interesting to observe that the relative importance of the different parts remains constant, while both resolved and SGS dissipation continue to increase or decrease, following the physical time oscillations of the DNS solution.

Even starting from the same threshold ϵ_0, the different SCALES solutions are able to adjust automatically and converge towards a certain thresholding level that increases with $\mathscr{R}_0$, while the grid compression increases as the number of active wavelets decreases. The time evolution of thresholding level ϵ for the different goal values is depicted in figure 15. With the increase of resolution, the SGS contribution to total dissipation decreases, corresponding to the decrease of the magnitude of the SGS kinetic energy (3.4). The one-to-one correspondence between prescribed resolution and SGS to resolved energy ratio is demonstrated by the plots shown in figure 16, confirming how this quantity could be assumed as an alternative *turbulence resolution* parameter, as discussed in § 4. Finally, as an example of high-order statistics, the skewness of a velocity derivative is depicted for the different SCALES solutions with time-varying thresholding in figure 17. The good performance of the self-adaptive method is maintained, regardless of the prescribed accuracy.

The results obtained for SCALES with different prescribed resolutions are summarized in table 2, by reporting some interesting time-averaged quantities. As expected, for increasing resolution, the time-averaged thresholding level decreases and the number of retained wavelets increases. As usual, the percentage of active wavelets

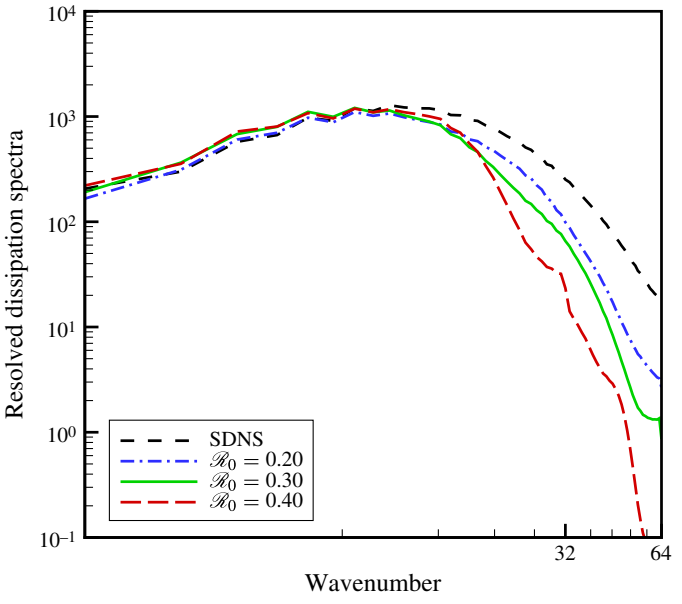

FIGURE 14. (Colour online) Time-averaged resolved dissipation spectra for SCALES with time-varying thresholding and different prescribed resolutions ($\mathscr{R}_0 = 0.20$, 0.30 and 0.40). The reference SDNS solution is shown for comparison.

$\mathscr{R}_0$	ϵ	% wavelets	$\mathscr{K}_{sgs}/\mathscr{K}_{res}$
0.20	0.21	2.68	0.037
0.30	0.33	0.86	0.053
0.40	0.44	0.37	0.078
0.50	0.49	0.20	0.124

TABLE 2. Time-averaged thresholding level, percentage of active wavelets, and SGS to resolved energy ratio for SCALES with different prescribed resolutions.

is suitably evaluated with respect to the maximum available number of wavelets (or, equivalently, grid points), that is, 256^3. When making a useful comparison with the reference SDNS grid that consists of 192^3 computational modes, the percentage of wavelets increases by a factor of 2.37, so that, for instance, it becomes 0.90 % for $\mathscr{R}_0 = 0.40$. The grid compression, however, remains very high, as usually happens for wavelet-based numerical methods (e.g. De Stefano *et al.* 2008).

To test the robustness and stability of the time-varying thresholding strategy, the following experiment is performed. Once a given resolution has been achieved, the goal value for $\mathscr{R}$ is changed to assess whether the solution automatically adjusts to the new level of prescribed resolution and (if it does) how long it takes. Two different experiments are conducted by altering the goal value from $\mathscr{R}_0 = 0.20$ to 0.40 and vice versa at a given non-dimensional time instant, $t \cong 10$. As illustrated in figure 18, the SCALES simulation with a threshold that is variable in time is able to react to the sudden modification by tending towards a new steady solution that corresponds to a different thresholding level. In both cases, a new balance between resolved and

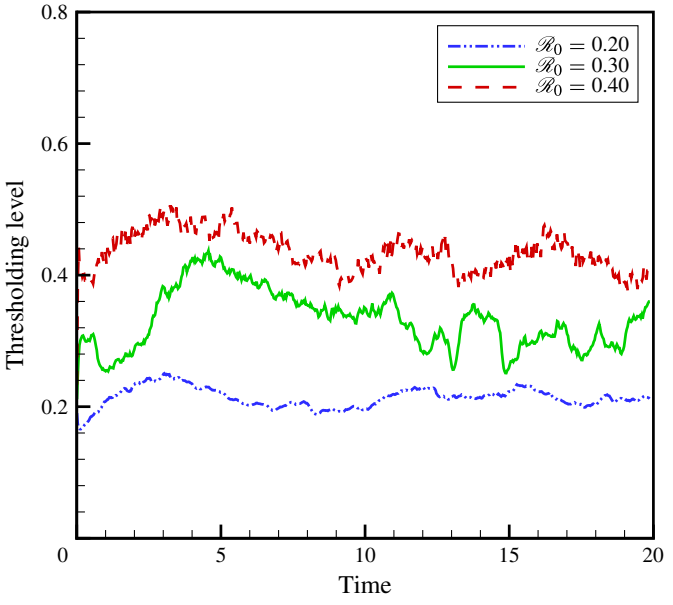

FIGURE 15. (Colour online) Time history of thresholding level for SCALES with time-varying thresholding and different prescribed resolutions ($\mathscr{R}_0 = 0.20$, 0.30 and 0.40).

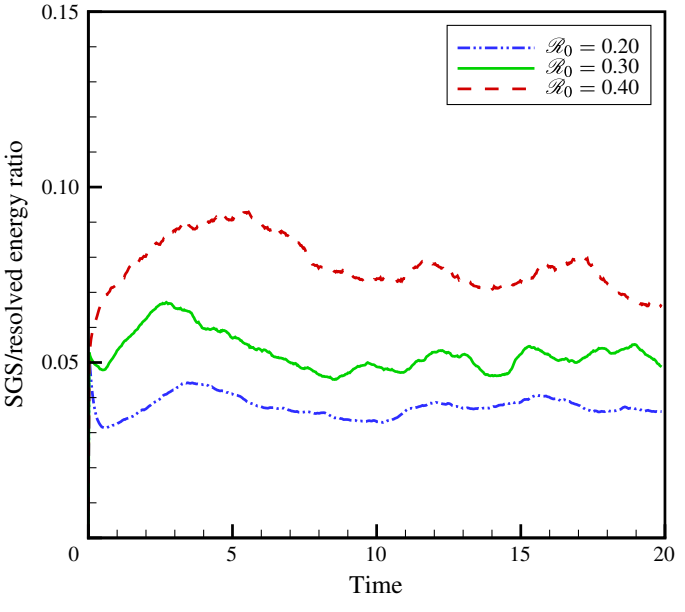

FIGURE 16. (Colour online) Time history of SGS to resolved energy ratio for SCALES with time-varying thresholding and different prescribed resolutions ($\mathscr{R}_0 = 0.20$, 0.30 and 0.40).

modelled dissipation is achieved, corresponding to the new prescribed goal, as clearly illustrated in figure 19.

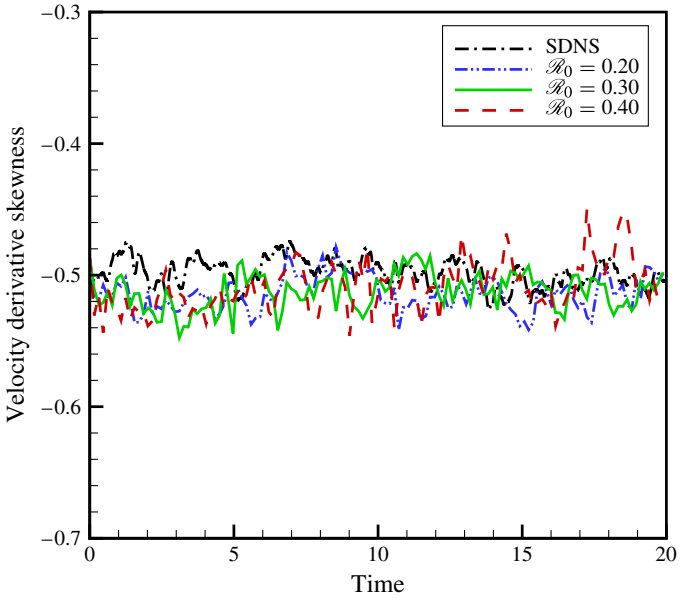

FIGURE 17. (Colour online) Resolved velocity derivative skewness for SCALES with time-varying thresholding and different prescribed resolutions ($\mathscr{R}_0 = 0.20$, 0.30 and 0.40). The reference SDNS solution is shown for comparison.

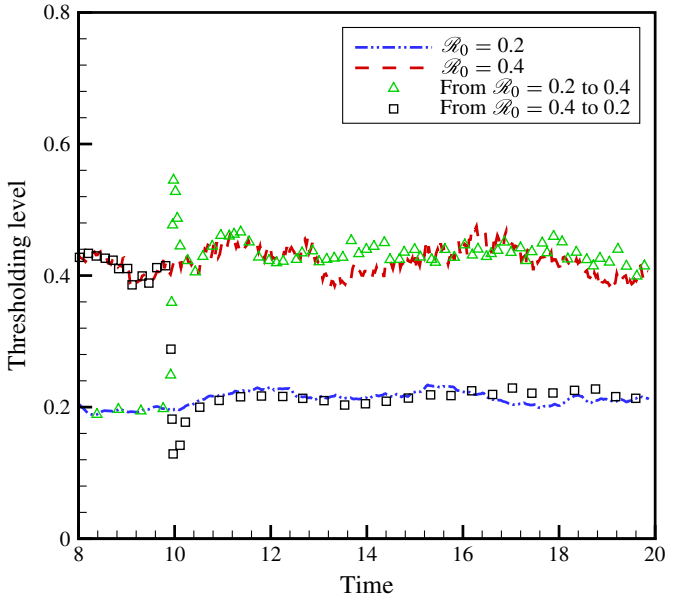

FIGURE 18. (Colour online) Time history of thresholding level for SCALES with time-varying thresholding and different prescribed resolutions modified at $t \cong 10$ (from $\mathscr{R}_0 = 0.20$ to 0.40, and vice versa).

It is worth noting that the transition between the two different steady conditions is very sharp in either case of coarsened or refined wavelet collocation grid. The characteristic time scale of the readjustment is much shorter than the eddy turnover

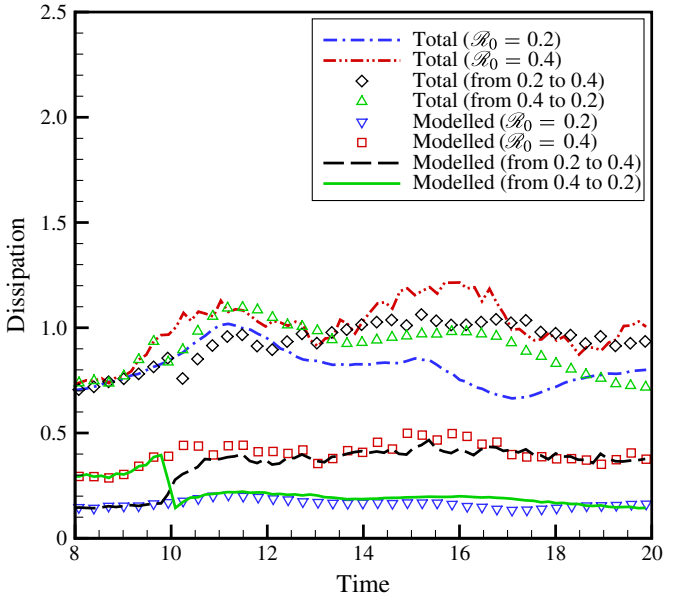

FIGURE 19. (Colour online) Modelled/total dissipation for SCALES with time-varying thresholding and different prescribed resolutions modified at $t \cong 10$ (from $\mathscr{R}_0 = 0.20$ to 0.40, and vice versa).

time of the turbulence, which confirms the validity of definition (4.3) for the relaxation parameter in the control equation (4.2). Owing to this fact, the present method can be reasonably applied to simulate statistically non-stationary turbulent flows.

Thus, in order to completely demonstrate the robustness of the proposed time-varying thresholding strategy, freely decaying turbulence is simulated by setting to zero the forcing term in the filtered momentum equation (3.2). The numerical experiments are conducted starting with the same initial condition as in the forced case, until the energy content of the flow becomes about one-tenth of the initial value. Two different resolutions are prescribed corresponding to the goal values $\mathscr{R}_0 = 0.20$ and 0.30, while starting with initial thresholding levels that ensure the desired resolution for the initial velocity field. Even in this case, a fully de-aliased pseudo-spectral 192^3 DNS solution is carried out as reference (SDNS).

When showing the results for decaying turbulence, the time variable is adimensionalized by the initial eddy turnover time corresponding to the reference SDNS solution. As illustrated in figure 20, the method is able to automatically adjust the thresholding parameter during the simulations while maintaining the desired values of *turbulence resolution*. For a given accuracy, as expected, the level of thresholding tends to increase as the turbulence decays. Both resolved and modelled dissipation decrease in time, while the total dissipation resembles the viscous dissipation of the reference SDNS. That is clearly shown in figure 21, where the different contributions to total dissipation, non-dimensionalized by the initial SDNS dissipation, are presented.

6. Concluding remarks

The actual value of wavelet thresholding level in wavelet-based numerical simulation of turbulence directly controls the relative importance of SGS modelling as well as

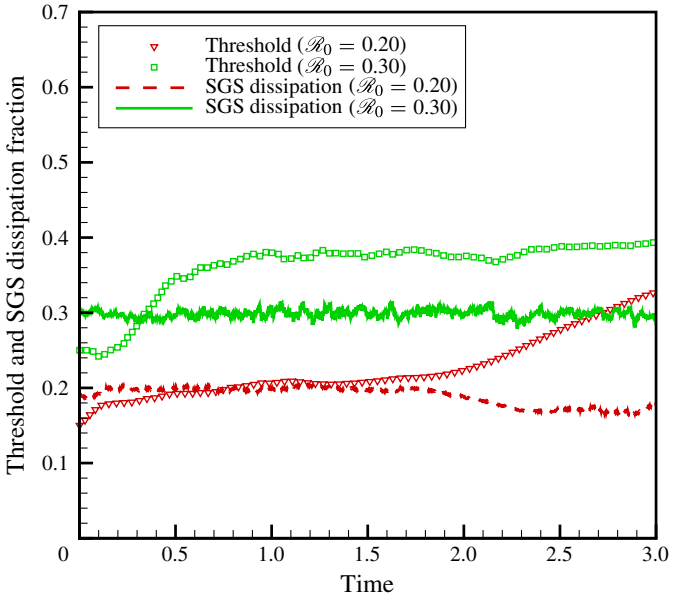

FIGURE 20. (Colour online) Time history of thresholding level and SGS dissipation fraction for SCALES with time-varying thresholding and two different prescribed resolutions ($\mathscr{R}_0 = 0.20$ and 0.30) in the decaying case.

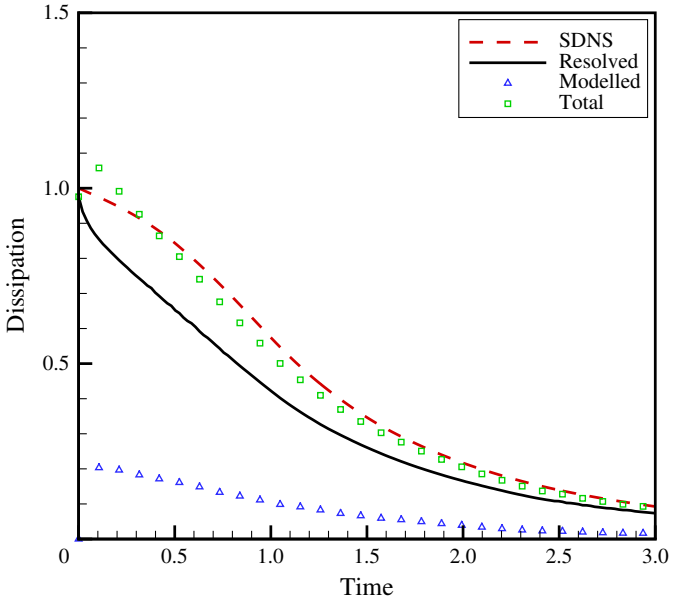

FIGURE 21. (Colour online) Modelled/total dissipation for SCALES with time-varying thresholding and prescribed resolution ($\mathscr{R}_0 = 0.20$) in the decaying case.

computational cost. The systematic study of the effect of varying this fundamental parameter has been conducted, while unequivocally defining the range of thresholds that allow for effective and efficient adaptive large eddy simulation.

A time-varying thresholding strategy, completely integrated with the localized dynamic energy-based model, has been introduced. In contrast to previous wavelet-based approaches, the present methodology does not presume any subjective choice for the wavelet thresholding level. The main outcome is in the possibility to perform adaptive *variable-fidelity* simulations of turbulent flows by simply prescribing the desired *turbulence resolution*, which can be expressed, for instance, in terms of the ratio of modelled to total dissipation.

The present work must be considered as the decisive step towards the development of a fully adaptive LES approach to the numerical simulation of steady/unsteady homogeneous turbulent flows. In this study, a number of numerical experiments have been successfully conducted for both linearly forced and freely decaying homogeneous turbulence at moderate Reynolds number. For unsteady turbulence, the thresholding level properly varies following the decaying nature of the flow, while maintaining the given level of *turbulence resolution*. The advantage of using a time-varying thresholding strategy is expected to be even more important when dealing with flows at realistic Reynolds numbers, where the energy-containing range is well separated from the dissipation range.

Finally, this study helps to address the complicated interconnections that exist in wavelet-based methods between filtering, closure modelling and numerics. In particular, it enhances the knowledge about the strong interaction between wavelet compression and modelled turbulent dissipation in wavelet-based simulations of turbulent flows.

Acknowledgements

This work was supported by the Department of Energy (DOE) under grant No. DE-FG02-07ER64468 and the National Science Foundation (NSF) under grant No. CBET-0756046. In addition, G.D. was partially supported by a grant from the Italian Ministry of Foreign Affairs (Selected Joint Mobility Project for the Exchange of Researchers between Italy and United States of America).

REFERENCES

DE STEFANO, G., GOLDSTEIN, D. E. & VASILYEV, O. V. 2005 On the role of sub-grid scale coherent modes in large eddy simulation. *J. Fluid Mech.* **525**, 263–274.

DE STEFANO, G. & VASILYEV, O. V. 2010 Stochastic coherent adaptive large eddy simulation of forced isotropic turbulence. *J. Fluid Mech.* **646**, 453–470.

DE STEFANO, G., VASILYEV, O. V. & GOLDSTEIN, D. E. 2008 Localized dynamic kinetic energy-based models for stochastic coherent adaptive large eddy simulation. *Phys. Fluids* **20** (4), 045102.

DONOHO, D. L. & JOHNSTONE, I. M. 1994 Ideal spatial adaptation via wavelet shrinkage. *Biometrika* **81**, 425–455.

FARGE, M., SCHNEIDER, K. & KEVLAHAN, N. 1999 Non-Gaussianity and coherent vortex simulation for two-dimensional turbulence using an adaptive orthogonal wavelet basis. *Phys. Fluids* **11** (8), 2187–2201.

GEURTS, B. J. & FRÖHLICH, J. 2002 A framework for predicting accuracy limitations in large-eddy simulation. *Phys. Fluids* **14** (6), L41–L44.

GHOSAL, S., LUND, T. S., MOIN, P. & AKSELVOLL, K. 1995 A dynamic localization model for large-eddy simulation of turbulent flows. *J. Fluid Mech.* **286**, 229–255.

GOLDSTEIN, D. E. & VASILYEV, O. V. 2004 Stochastic coherent adaptive large eddy simulation method. *Phys. Fluids* **16** (7), 2497–2513.

GOLDSTEIN, D. E., VASILYEV, O. V. & KEVLAHAN, N. K. R. 2005 CVS and SCALES simulation of 3D isotropic turbulences. *J. Turbul.* **6** (37), 1–20.

HASELBACHER, A. & VASILYEV, O. V. 2003 Commutative discrete filtering on unstructured grids based on least-squares techniques. *J. Comput. Phys.* **187** (1), 197–211.

KEVLAHAN, N. K. R. & VASILYEV, O. V. 2005 An adaptive wavelet collocation method for fluid–structure interaction at high Reynolds numbers. *SIAM J. Sci. Comput.* **26** (6), 1894–1915.

LUNDGREN, T. S. 2003 Linearly forced isotropic turbulence. In *Annual Research Briefs, Center for Turbulence Research*, pp. 461–473. Stanford University.

MACHIELS, L. 1997 Predictability of small-scale motion in isotropic fluid turbulence. *Phys. Rev. Lett.* **79**, 3411–3414.

MARSDEN, A. L., VASILYEV, O. V. & MOIN, P. 2002 Construction of commutative filters for LES on unstructured meshes. *J. Comput. Phys.* **175**, 584–603.

MEYERS, J. & SAGAUT, P. 2006 On the model coefficients for the standard and the variational multi-scale Smagorinsky model. *J. Fluid Mech.* **569**, 287–319.

POPE, S. 2004 Ten questions concerning the large-eddy simulation of turbulent flows. *New J. Phys.* **6**, 1–24.

ROSALES, C. & MENEVEAU, C. 2005 Linear forcing in numerical simulations of isotropic turbulence: physical space implementations and convergence properties. *Phys. Fluids* **17**, 1–8.

SAGAUT, P., DECK, S. & TERRACOL, M. 2006 *Multiscale and Multiresolution Approaches in Turbulence*. Imperial College Press.

SCHNEIDER, K. & VASILYEV, O. V. 2010 Wavelet methods in computational fluid dynamics. *Annu. Rev. Fluid Mech.* **42**, 473–503.

TERRACOL, M., SAGAUT, P. & BASDEVANT, C. 2003 A time self-adaptive multilevel algorithm for large-eddy simulation. *J. Comput. Phys.* **184**, 339–365.

VASILYEV, O. V. 2003 Solving multi-dimensional evolution problems with localized structures using second generation wavelets. *Intl J. Comput. Fluid Dyn.* **17** (2), 151–168.

VASILYEV, O. V. & BOWMAN, C. 2000 Second generation wavelet collocation method for the solution of partial differential equations. *J. Comput. Phys.* **165**, 660–693.

VASILYEV, O. V., DE STEFANO, G., GOLDSTEIN, D. E. & KEVLAHAN, N. K. R. 2008 Lagrangian dynamic SGS model for stochastic coherent adaptive large eddy simulation. *J. Turbul.* **9** (11), 1–14.

VASILYEV, O. V. & KEVLAHAN, N. K. R. 2005 An adaptive multilevel wavelet collocation method for elliptic problems. *J. Comput. Phys.* **206** (2), 412–431.

VASILYEV, O. V., LUND, T. S. & MOIN, P. 1998 A general class of commutative filters for LES in complex geometries. *J. Comput. Phys.* **146**, 105–123.

VINCENT, A. & MENEGUZZI, M. 1991 The spatial structure and statistical properties of homogeneous turbulence. *J. Fluid Mech.* **225**, 1–20.